JOURNAL OF PHYSICAL ORGANIC CHEMISTRY
J. Phys. Org. Chem. 2006; **19:** 148–156
Published online in Wiley InterScience (www.interscience.wiley.com). DOI: 10.1002/poc.1000

Study of a potential inhibitor of acetylcholinesterase using UV spectrophotometry, NMR spectroscopy and molecular modeling

Isabelle Correia,[1]* Nello Ronzani,[1] Nicole Platzer,[2] Bich-Thuy Doan[2] and Jean-Claude Beloeil[2]

[1]Structure et Fonction de Molécules Bioactives (UMR 7613), UPMC Paris 6, BP 45, 4 Place Jussieu, 75252 Paris Cedex 05, France
[2]Laboratoire de RMN Biologique, ICSN, CNRS, Avenue de la Terrasse, 91198 Gif-sur-Yvette Cedex, France

Received 17 December 2004; revised 14 September 2005; accepted 23 September 2005

ABSTRACT: 1-[6-(Acridine-9-carbonyloxy)hexyl]pyridinium chloride (**1**) was synthesized and studied as a potential inhibitor of acetylcholinesterase (AChE), which is frequently involved in Alzheimer's disease. UV spectrophotometry showed that **1** is a reversible and competitive inhibitor of AChE ($K_i \approx 2 \times 10^{-7}$ M). NMR (TrNOESY) showed that **1**, bonded to AChE, maintains an extended form that allows hydrophobic interactions to occur between the aliphatic chain and the deep and narrow gorge of AchE and favors interactions between the acridine group and the catalytic and anionic subsites situated at the bottom of the gorge, and also between the pyridinium ring and the peripheral site. A more detailed picture of the structure of the complex was obtained by combining NMR structural data and molecular modeling (docking, dynamics simulation and energy calculations). Copyright © 2006 John Wiley & Sons, Ltd.
Supplementary electronic material for this paper is available in Wiley Interscience at http://www.interscience.wiley.com/jpages/0894-3230/suppmat/

KEYWORDS: acetylcholinesterase inhibitor; 1-[6-(acridine-9-carbonyloxy)hexyl]pyridinium chloride; UV; NMR; dynamics; molecular modeling

INTRODUCTION

Previous laboratory studies have shown that esters of the type $RCOO(CH_2)_nC_6H_5N^+\ Cl^-$ are competitive inhibitors of cholinesterases and have an anticholinesterase activity similar to that of physostigmine. 1-[6-(Acridine-9-carbonyloxy)hexyl] pyridinium chloride (**1**) was chosen to evaluate the anticholinesterase activity of this type of molecule for several reasons. Acridine is itself a significant inhibitor of acetylcholinesterase (AChE).[1] The functional groups of **1**, the 9-substituted acridine and pyridinium, are likely to interact with various sites of the enzyme. Sussman *et al.*[2] established the crystallographic structure of *Torpedo californica* AChE. The catalytic site comprises the triad of amino acids Ser^{200}, His^{440} and Glu^{327}. It is situated at the bottom of a deep and narrow gorge densely lined by aromatic residues. Near the bottom of the gorge, a secondary site, namely the anionic subsite, includes in particular Trp^{84}. At the opening of the gorge, a peripheral site comprises Tyr^{70}, Phe^{290} and Trp^{279}. There are thus several different sites at which the various elements of an inhibitor can bind to AChE. For example, molecular modeling has shown that in the complex formed with *N*-monoalkylated derivatives of 9-amino-1,2,3,4-tetrahydroacridine, the planar tacrine moiety (THA) is sandwiched between Phe^{330} and Trp^{84}, while the alkylene chain is aligned within the gorge.[3] Compounds bearing functional groups such as a carbonyl or a carbamate have been shown to act as inhibitors.[1,4] On the basis of the crystallographic structure of *Torpedo californica* AChE,[2] a dual binding site mode has been shown to occur with dimers bearing quaternary groups, e.g. decamethonium, edrophenium.[5] In addition to the catalytic site, the peripheral site is also involved and Trp^{279} appears to interact with quaternary groups that have a permanent positive charge. A study of alkylene-linked bis-THA has shown that it has much greater inhibitor potency than the monomer, provided that the spacer between quaternary groups is long enough. An aliphatic chain with seven methylene groups best satisfies this requirement.[6] The association of a tacrine unit and of a 5-amino-5,6,7,8 tetrahydro-2(1*H*)-quinolinone unit to form a hybrid akylene-linked inhibitor results in high AChE inhibition potency and selectivity with respect to butyrylcholinesterase (BchE).[7]

In **1**, both the acridine ring system and the pyridinium are able to interact with the binding sites of AChE. The acridine ring nitrogen or the carbonyl might be involved in a hydrogen bonding interaction. Taking into account the COO group linked to the hexamethylene chain, the tether length is nearly equivalent to that in the heptamethylene-linked tacrine dimer.[8]

**Correspondence to:* I. Correia, Structure et Fonction de Molécules Bioactives (UMR 7613), UPMC Paris 6, Bât F, BP 45, 4 Place Jussieu, 75252 Paris Cedex 05, France.
E-mail: correia@ccr.jussieu.fr

An alternative to using molecular modeling to gain information on the molecular form of an inhibitor linked to AChE is to use NMR transferred NOE from the bonded inhibitor to the free inhibitor.[9] Compound **1** was found to meet the stringent conditions required. In the context of a slow exchange and with a small fraction of the ligand in the bound state, the exchange rates were fast enough to transfer the cross-relaxation pathways in the AChE–ligand complex to the free ligand resonances.

RESULTS AND DISCUSSION

Synthesis

Compound **1** was synthesized according to the usual procedure (Scheme 1),[10–12] and was characterized by ^{1}H and ^{13}C NMR spectroscopy in D_2O solution (see NMR study). The pK_a* (uncorrected for the deuterium isotope effect) of **1**, determined in D_2O solution by ^{1}H NMR spectroscopy, was 3.6.

Anticholinesterase activity

UV spectrophotometry was used to compare the anticholinesterase activities of **1** and acridine. The enzymatic activity of electric eel AChE was measured using the Ellman method.[13] The substrate, S, is acetylthiocholine iodide. The hydrolysis product reacts with added 5,5′-dithiobis(2-nitrobenzoic acid) (DTNB) which is instantaneously converted to 5-thio-2-nitrobenzoate anion. The absorbance, A_0, of the 5-thionitrobenzoate anion was measured as a function of time at $\lambda_{max} = 412$ nm ($\varepsilon = 13\,600\ M^{-1}\,cm^{-1}$). For each substrate

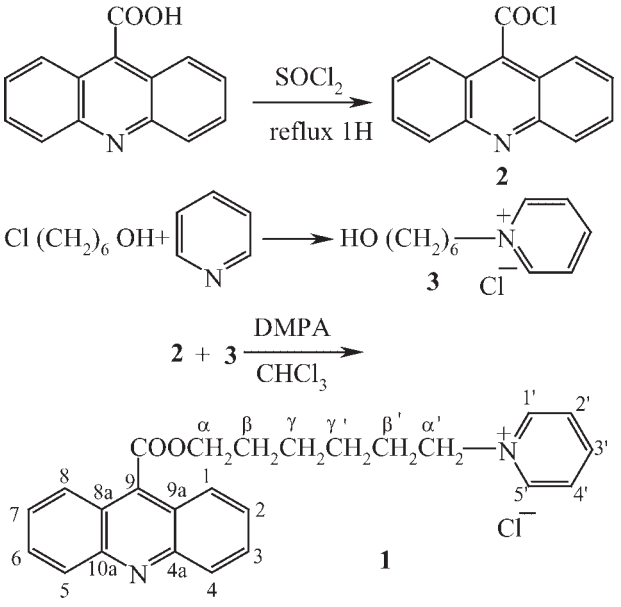

Scheme 1

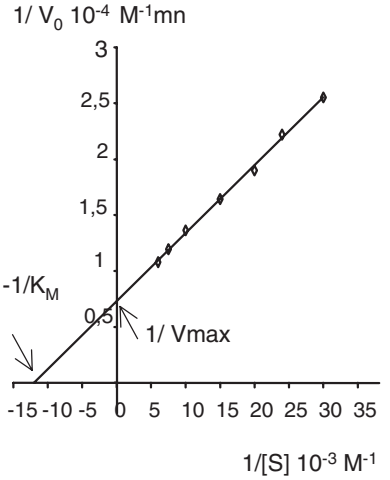

Figure 1. Lineweaver–Burk plot for AChE–acetylthiocholine (S)

concentration, the initial velocity, V_0, of the enzymatic reaction was obtained from the initial slope of the curve $A_0 = f(t)$. The maximum velocity, V_{max}, and the Michaelis–Menten constant, K_M,[14] are best deduced from a double reciprocal plot of the enzyme kinetics, $1/V_0$, as a function of 1/[S] (Lineweaver–Burk plot).[15] The mean value of K_M for AChE–acetylthiocholine was $(0.85 \pm 0.11) \times 10^{-4}$ M (11 independent measurements) (Fig. 1).

Measurement of the rate of catalysis for different concentrations of inhibitor makes it possible to distinguish between non-competitive and competitive inhibition.[16] In non-competitive inhibition, the intercept on the *y*-axis of the Lineweaver–Burk plot is increased when the inhibitor is added, whereas in competitive inhibition it remains the same in the presence and absence of inhibitor (Fig. 2). For a competitive inhibitor, the slope of the straight line is increased by a factor of $1 + [I]/K_I$, where [I] is the inhibitor concentration and K_I the dissociation constant of the enzyme–inhibitor complex.

The IC_{50} value of the inhibitor studied was determined graphically by plotting the percentage inhibition, $100(V_0 - V_i)/V_i$, as a function of [I] at a constant substrate

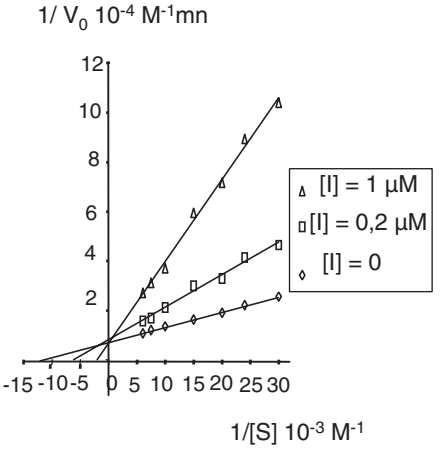

Figure 2. Lineweaver–Burk plot for AChE–acetylthiocholine in the absence ($I = 0$) or presence of **1** ($I = 0.2$ and 1 µM)

Table 1. Inhibition of acetylcholinesterase (from electric eel) by **1**, acridine and some acridine derivatives (substitution at position 9)

Compound	IC_{50} (μM)	$K_i \pm 20\%$(μM)	Log$P \pm 0.3$
1-[6-(Acridine-9-carbonyloxy)hexyl]pyridinium chloride (**1**)	0.60	0.2	0.76[a]
6-Chlorohexyl-9-acridine carboxylate (**4**)	30	10	5.89[a]
Acridine	60	17	3.41[a]
9-Amino-1,2,3,4 tetrahydroacridine (tacrine)	0.223 ± 0.011[c]	0.01	3.30[b]
9-Aminoacridine (aminacrine)	0.21	0.07	2.74[b]

[a]Log*P* (octanol–water partition coefficient) was evaluated with ACD/LogP Prediction software.
[b]Ref. 17.
[c]Ref. 7.

concentration [S] chosen to ensure a value of V_0 approximating to V_{max} in the absence of inhibitor.

Finally, the reversibility of the inhibition produced by **1** was checked by means of the dilution test. The reaction velocity, $\Delta A_0\,min^{-1}$, was measured without inhibitor before and after diluting by a factor of 10. The values were 2 and 0.17, respectively. In the presence of inhibitor at IC_{50}, the reaction velocities found before and after dilution were much less different, 0.75 and 0.11, respectively. These results demonstrate the reversibility of the inhibition.

Data characteristic of the inhibition of AChE by **1**, acridine and various derivatives are reported in Table 1.

The UV spectrophotometric study clearly shows that **1** is a reversible and competitive inhibitor of AChE. Comparison of **1** with **4** demonstrated the important role played by the pyridinium group.

It is highly likely that an interaction occurs with the enzyme in the dual binding site mode. The acridine group in **1** probably allows, like acridine itself, good insertion into the hydrophobic pocket in the vicinity of the anionic site and the charged pyridinium group interacts with Trp^{279}. The binding efficiency of **1** is similar to that of good inhibitors currently being tested, such as physostigmine ($K_i = 0.27$ μM) and heptylphysostigmine ($K_i = 0.1$ μM),[4,18] and approaches that of tacrine ($K_i = 0.01$ μM), a drug in use for Alzheimer's disease.

NMR study of 1-[6-(acridine-9-carbonyloxy) hexyl]pyridinium chloride (1)

In the ^1H spectrum, the AA′XX′M spin system of the pyridinium ring is clearly distinguished from the first-order spin system of the acridine group (Fig. 3). The six methylene groups give distinct signals. Univocal assignments require it to be possible to distinguish between the

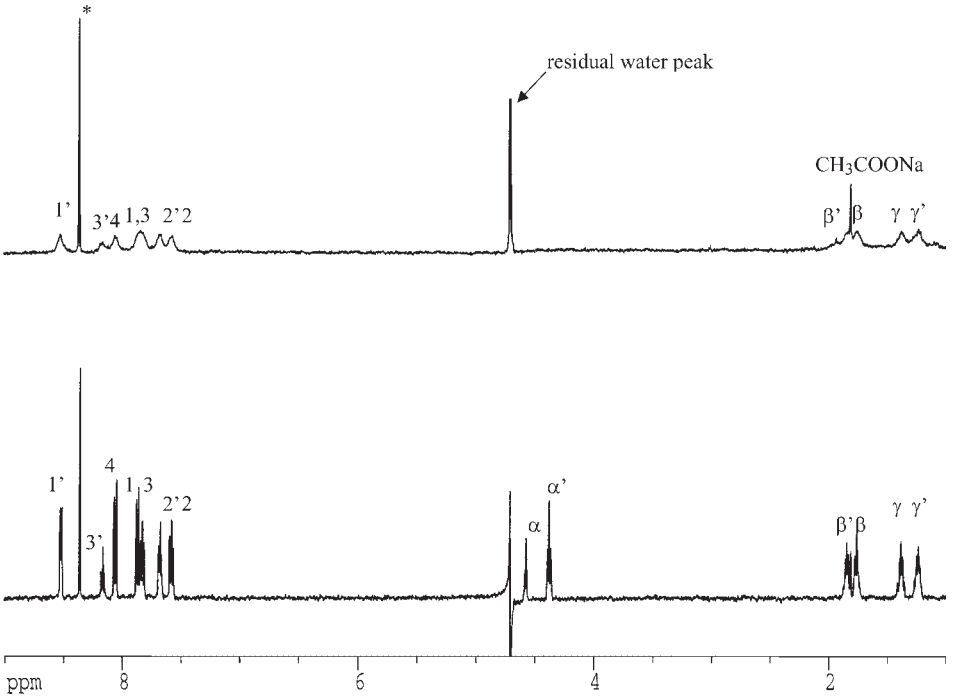

Figure 3. 1D ^1H NMR spectra of (bottom) free ligand **1** (1 mM) and (top) the ligand **1** in the presence of AChE (15 μM) in phosphate buffer (pH* = 7.4, 298 K). The significant line broadening observed in the presence of the enzyme indicates binding of the small molecule. In the presence of AChE, α and α' signals have disappeared owing to strong broadening. The peak marked with an asterisk is due to an impurity coming from HPLC (sodium formate)

signals of H1, H8 and H4, H5 and between the signals of the α and α' methylene groups. Through a NOESY experiment, the proximity between the acridine protons at 7.95 ppm and the aliphatic protons at 4.66 ppm was clearly demonstrated, making it possible to assign the corresponding signals to H1, H8 and to the α-methylene of the chain respectively (see Supplementary material, available in Wiley Interscience). The assignments of the other protons were then obtained by use of a 2D COSY experiment. The assignments of the ^{13}C resonances were finally deduced from ^{13}C–^{1}H correlations on the basis of 2D HSQC and HMBC experiments. Data are reported in Table 2.

The values of the ^{3}J coupling constants measured for the methylene protons indicate an extended conformation, and this was further confirmed by the dipolar interactions detected in the NOESY map between Hα and Hγ and between Hα' and Hγ'. Finally, dipolar interactions were found to be less intense between H1, H8 and Hα than between H1, H8 and Hβ or Hγ. Hence the Cα in the alkyl chain appeared to be located in the *s-cis* position with respect to the carbonyl in its preferred conformation.

The chemical shifts of the various protons in **1** depend on the concentration. This effect, which is more marked for the protons of the acridine group, decreases within the chain from the α to the α' position and finally becomes insignificant for the protons of the pyridinium group. These data suggest a dimerization of **1**, involving the stacking of the acridine groups and a head-to-tail disposition of the two molecules. The dimerization constant determined by ^{1}H NMR spectroscopy and by concentration curve fitting nevertheless had a low value, $39 \pm 10\,M^{-1}$ at 296 K, and the monomer remains the predominant form.

NMR study of the interaction between AChE and compound 1

NMR spectroscopy is widely used to study enzyme–substrate and enzyme–inhibitor interactions in solution. Among the NMR parameters, chemical shift, linewidth and relaxation times are those most likely to undergo significant changes. Since in the present case the molecular weights of the enzyme and of the inhibitor are very high ($\sim$260 kDa) and low (420.5 Da), respectively, the correlation times are very different (ca 10^{-7} and 10^{-10} s, respectively). This means that in the ^{1}H NMR spectrum recorded for an enzyme–inhibitor mixture, the resonances of the enzyme are not observed, whereas those of the ligand are easily detected. Nevertheless, according to the Swift and Connick relation,[19] significant broadening is expected for the signals of the ligand L when it complexes:

$$\pi\Delta\nu = \frac{1}{T_2^{obs}} = \frac{1}{T_2^{F}} + \frac{f^{C}}{\tau^{C}} \times \left[\frac{\frac{1}{T_2^{C}}\left(\frac{1}{T_2^{C}} + \frac{1}{\tau^{C}}\right) + (\Delta\omega^{C})^2}{\left(\frac{1}{T_2^{C}} + \frac{1}{\tau^{C}}\right)^2 + (\Delta\omega^{C})^2} \right]$$

where the exponents F and C indicate the free and bound states, respectively, $\Delta\nu$ the width at half-height in the

Table 2. 1-[6-(Acridine-9-carbonyloxy)hexyl]pyridinium chloride (**1**) (1.2×10^{-3} M) in D_2O: ^{1}H NMR chemical shifts and coupling constants and ^{13}C NMR chemical shifts

Site	^{1}H δ (ppm)[a]	^{1}H $\Delta\delta$ (ppm)[b]	J(H,H) (Hz $\pm$ 0.3)	^{13}C δ (ppm)[c]
1–8	7.95	−0.34	$J(1,2) = J(8,7) = 8.7$ $J(1,3) = J(8,6) = 2.1$ $J(1,4) = J(8,5) = 1.3$	124.91
2–7	7.66	−0.27	$J(2,3) = J(7,6) = 6.6$ $J(2,4) = J(7,5) = 1.2$	128.02
3–6	7.90	−0.25	$J(3,4) = J(6,5) = 8.8$	131.95
4–5	8.14	−0.31		128.06
4a, 10a				147.89
9				137.94
9a, 8a				122.02
CO				169.18
α	4.66	−0.23	$J(\alpha,\beta) = 6.2$	68.20
β	1.85	−0.20	$J(\beta,\gamma) = 7.3$	27.41
γ	1.47	−0.20	$J(\gamma,\gamma') = 7.5$	25.25
γ'	1.33	−0.20		25.12
β'	1.93	−0.15	$J(\beta',\gamma') = 7.5$	30.19
α'	4.46	−0.10	$J(\alpha',\beta') = 7.2$	61.93
1′–5′	8.60	−0.06	—	144.00
2′–4′	7.75	0.0	—	127.97
3′	8.24	−0.01	$J(3',2') = J(3',4') = 7.8$ $J(3',1') = J(3',5') = 1.4$	145.47

[a]Referenced to DSS (0 ppm) at 296 K.
[b]Chemical shift variation with increased concentration (from 1.2×10^{-3} to 10.2×10^{-3} M).
[c]Referenced to DSS (0 ppm) at 296 K.

absence of coupling interaction, $f^C = [L^C]/[L^T]$ the molar ratio of bound ligand, $[L^T]$ the total concentration, $\Delta\omega^C = \omega^C - \omega^F$ the angular frequency change after complexing, τ^C the life time in bound state and $1/T_2{}^F$ and $1/T_2{}^C$ the relaxation rates. This equation is valid if $[L^C] < [L^F]$.

Comparison of the spectra of **1**, recorded in the absence and presence of AChE (15 μM active sites), clearly shows that all the signals were significantly broadened in the latter case (Fig. 3). In contrast, the chemical shifts showed no significant change, owing to the very low fraction of bound ligand.

The widening of the signals in itself is not sufficient to demonstrate whether the frequency of the exchange between the free and bound ligand is rapid, intermediate or slow. Nevertheless, when the dissociation constant has a low value, as is the case for the complex AChE–**1** ($\sim 2 \times 10^{-7}$ M as estimated by UV spectrophotometry), the exchange is slow on the frequency scale.[20,21] The spectrum of **1** (1 mM) in the presence of AChE (2.24 μM active sites) was recorded as a function of temperature (Fig. 4). Since the linewidth increases when the temperature increases, the exchange is indeed in the slow domain. In this experiment, changes in chemical shifts resulted from the decrease in the dimerization constant of free ligand **1**.

Further valuable information was obtained using the NOE transfer experiment, which demonstrates the interaction of a ligand with a macromolecular system and provides 3D structural data for the ligand. The need for such an investigation is the rapid exchange on the relaxation rates scale. In order to reduce the contribution of the intramolecular NOE within the free ligand and to minimize spin diffusion in the bound state, the mixing time used in the TrNOESY sequence was kept short (65 ms). In the presence of AChE, **1** in the bound state has a correlation time, τ_c, similar to that of the enzyme ($\omega\tau_c$ much greater than 1.12). Negative NOEs are then transferred by exchange from the bound ligand to the free ligand, correlations of which are observed in the TrNOESY map (see Supplementary material). As a result, the intra-ligand cross peaks and the diagonal peaks have the same sign. The qualitative NOE and TrNOE data are listed in Table 3. The cross peaks that result from interactions between Hα and Hγ and between Hα' and Hγ' and in contrast the lack of any cross peaks resulting from interactions between the pyridinium ring and the acridine motif, demonstrate that **1** maintains an extended conformation when it is bound to the enzyme. This conformation is required for the interaction with the enzyme to occur in the dual binding site mode.

Modeling of the interaction between AChE and compound 1

The molecular modeling protocol was as follows. The calculations were performed using the molecular

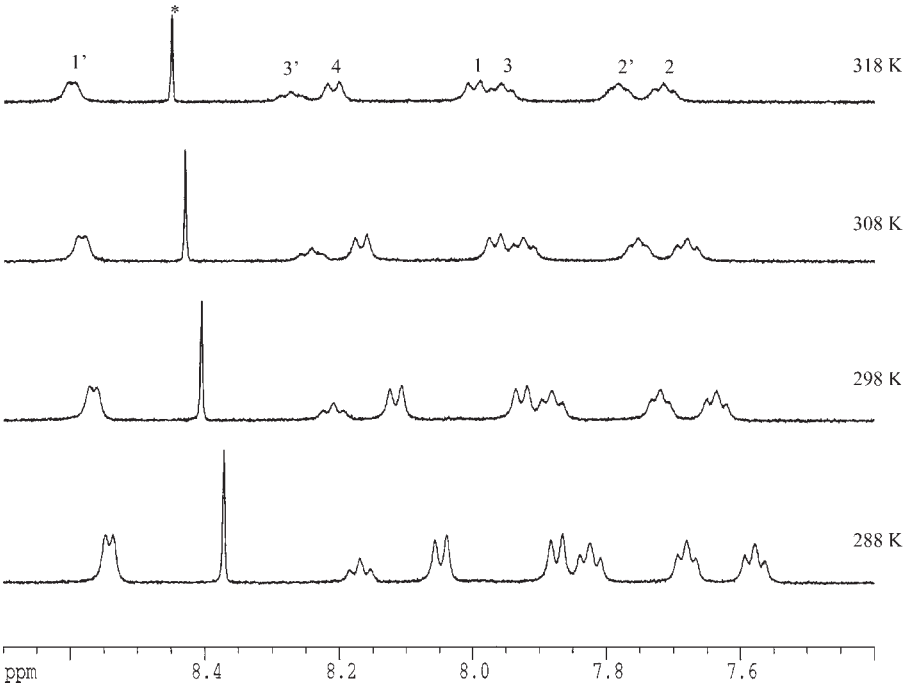

Figure 4. ^{1}H NMR spectra of the aromatic region of **1** (1 mM) in the presence of AChE (2.24 μM) in phosphate buffer (100 mM, pH* = 7.4) at different temperatures. The line broadening observed with increasing temperature indicates an exchange in the slow domain on the frequency scale between the free and bound ligand. The peak marked with an asterisk is due to an impurity coming from HPLC (sodium formate)

Table 3. Qualitative NOE and TrNOE data for 1-[6-(acridine-9-carbonyloxy)hexyl]pyridinium chloride (**1**) (1 mM) in the absence and presence of AChE in D_2O buffered solution

^{1}H observed	**1**: NOEs[a,b]	**1** in the presence of AChE: TrNOEs[b,c]
H1–H8	H2–H7 (s) Hα (m) Hβ (m) Hγ (m)	H2–H7 (s) Hβ (m) Hγ (w)
H2–H7	H1–H8 (s) H3–H6 (s)	H1–H8 (s) H3–H6 (s) H4–H5 (w*)
H3–H6	H2–H7 (s) H4–H5 (s)	H2–H7 (s) H4–H5 (s)
H4–H5	H3–H6 (s)	H3–H6 (s) H2–H7 (w*)
Hα	Hβ (s) Hγ (s) Hγ′ (w*)	Hβ (s) Hγ (m)
Hβ	Hα (s) Hγ (s) Hγ′ (s)	Hα (s) Hγ (s) Hγ′ (s)
Hγ	Hα (s) Hβ (s) Hβ′ (s) Hγ′ (s)	Hα (s) Hβ (s) Hβ′ (s) Hγ′ (s)
Hα′	Hβ′ (s) Hγ′ (s) Hγ (w*)	Hβ′ (s) Hγ′ (s) Hγ (w*)
Hβ′	Hα′ (s) Hγ′ (s) Hγ (s)	Hα′ (s) Hγ′ (s) Hγ (s)
Hγ′	Hα′ (s) Hβ′ (s) Hγ (s) Hβ (s)	Hα′ (w*) Hβ′ (s) Hγ (s) Hβ (s)
H1′–H5′	H2′–H4′ (s) Hα′ (s) Hβ′(s) Hγ′ (m)	H2′–H4′ (s) Hα′ (w*) Hβ′(m)
H2′–H4′	H1′–H5′ (s) H3′ (s)	H1′–H5′ (s) H3′ (s)
H3′	H2′–H4′ (s)	H2′–H4′ (s)

[a]Observed NOE data from 2D ^{1}H NOESY ($\tau_m = 1$ s, NOEs > 0) experiment at 303 K and pH* = 7.8. pH*: the pH value reported is the pH meter reading, uncorrected for the deuterium isotope effect.
[b]2–3 Å, s: strong, 3–4 Å, m: medium, 4–5 Å, w: weak. (w*: very weak).
[c]TrNOESY (**1**: AChE ratio = 446, $\tau_m = 65$ ms, TrNOEs < 0) experiment at 303 K and pH* = 7.8.

modeling software package SYBYL 6.5 (Tripos Associates, St. Louis, MO, USA) on a Silicon Graphics Indigo 2 Extreme workstation. The Tripos force field with a dielectric constant of 80 and a cutoff of 8 Å for the nonbonded interaction and electrostatic Gasteiger–Hückel charges for the ligand was applied.

The structure of the complex formed between AChE and **1** was calculated using standard computational procedures of docking, energy minimization (EM) and molecular dynamics (MD) simulation.

To initiate the docking stage, a refined structure of **1**, (EM and MD kept in a linear conformation), was superimposed on the (*S*,*S*)-(−)-bis(10)-hupyridone molecule, a neighboring ligand embedded in the binding active site of the *Torpedo californica* acetylcholinesterase, *Tc*AChE,[22] taken from the crystallographic structure of the complex (Brookhaven database, entry 1h22.pdb). The enzyme was kept as a rigid template and ligand **1** was anchored by superimposing the main axis of its structure extended linearly in coherence with the NMR TrNOESY data. The orientation of **1** was chosen from its hydrophobic and expected electrostatic affinity to the active and anionic peripheral site of the enzyme. It was positioned by defining constraints with distance range between 3 and 5 Å, with a force constant of 5 kcal^{-1} mol^{-1} Å^{-2} during the simulation. Despite the lack of experimental NOEs between the ligand and the enzyme, the constraints are defined as follows: on the one hand between the H2, H3, H4, H5 and H6 protons of the acridine ring and the aromatic protons of Trp^{84}, Phe^{330}and His^{440} at the bottom of the enzyme gorge, and on the other hand between the H1′, H2′, H3′ and H4′ of the pyridinium ring and the protons of Tyr^{70}, Phe^{290} and Trp^{279} at the peripheral site. Manual docking to choose an initial conformation of the inhibitor docked into the active site was performed where the enzyme was kept as a rigid template first outside a sphere of 20 Å.

From this model, a first step of EM was performed with 200 steps of steepest descent, 200 steps of conjugate gradient procedure. Repeated simulated annealing consisted in the dynamic molecular simulation procedure: 10 steps from 0 to 1000 K, 10 ps at 1000 K and decreasing to 300 K for 10 ps. This was followed by an energy minimization stage, with 250 steps of steepest descent, 250 steps of conjugate gradient procedure, followed by 1000 steps with the Powell method.

The resulting lowest energy molecules were kept and superimposed. Compound **1** embedded in the *Tc*AChE gorge displays a well-defined conformation represented by one mean structure (Fig. 5). It shows a 3D structure tightly bound and well fitted to the active and peripheral sites. The position of **1** appears stabilized by hydrophobic interactions between the aromatic protons of the acridine part and the aromatic protons of Phe^{330}, His^{440} and Trp^{84}of the *Tc*AChE catalytic and anionic subsites, respectively, and by hydrophobic interactions occurring between the cationic pyridinium part and the peripheral site, namely the amino acids Phe^{290}–Trp^{279}–Tyr^{70} (Trp^{279} is known to interact with cationic ligands). The C6 aliphatic chain perfectly fits into the gorge, extending from the active site toward the peripheral site.

The modeling of the complex provides a likely conformation of **1** that accords with the TrNOESY NMR results. It supports the likelihood of specific interactions involving a dual binding site of **1** with *Tc*AChE, which would account for the inhibition demonstrated by UV experiments.

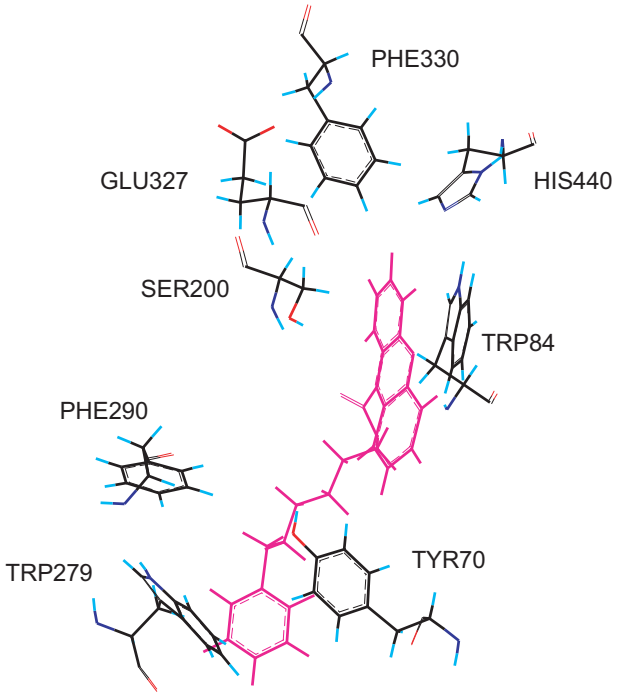

Figure 5. Favorable regions of interaction between **1** and *Tc*AChE. Near the bottom of the gorge of the enzyme, the planar acridine moiety is sandwiched between the rings of Phe^{330}, His^{440} and Trp^{84} localized in the catalytic and anionic subsites, respectively. The extended alkyl chain lines along the wall of the hydrophobic gorge. At the top of the gorge, the pyridinium moiety interacts with Trp^{279} in the peripheral binding site. Compound **1** is displayed in a stick representation

CONCLUSION

Using reversible inhibitors of AChE as drugs is one possible approach to alleviate the acetylcholine deficit associated with Alzheimer's disease. Among esters of type $RCOO(CH_2)_nC_6H_5N^+\,Cl^-$, we chose 1-[6-(acridine-9-carbonyloxy)hexyl]pyridinium chloride (**1**). Enzymatic assays using UV spectrophotometry showed that **1** is a reversible competitive inhibitor of AChE. It is more potent than 6-chlorohexyl-9-acridine carboxylate (**4**), which is devoid of the pyridinium ring (~50-fold), and than acridine alone (~100-fold). These findings suggest that **1** is bound to AChE in the dual binding mode frequently encountered for bifunctional inhibitors. One requirement for such an interaction to occur is an extended conformation of the ligand. An NMR NOESY study showed that in aqueous solution **1** fulfils this prerequisite. NMR transferred NOESY, an efficient way to obtain information about a ligand bound to an enzyme when it cannot be observed directly, demonstrated that **1** bound to AChE does indeed preserve an extended conformation. Computerized docking with dynamics simulation of **1** indicates likely binding sites and ligand orientation, with the acridine moiety anchored in the catalytic and anionic subsites and the pyridinium interacting with the peripheral site. The length of the tether would allow it to be aligned along the deep gorge between these sites.

EXPERIMENTAL

Chemical synthesis. 9-Acridinecarboxylic acid (1 g) was reacted with $SOCl_2$ (50 ml) under reflux for 1 h. The mixture was poured in water and extracted with diethyl ether to yield 9-acridinecarboxylic chloride (**2**). A solution of 6-chloro-1-hexanol (5 ml) in pyridine (20 ml) was refluxed for 5 h. After eliminating the pyridine under vacuum, 6-hydroxyhexyl-1-pyridinium chloride (**3**) was obtained in quantitative yield. Compound **2** (1.03×10^{-4} M) plus **3** (1.04×10^{-4} M) were dissolved in $CDCl_3$ (5 ml) and, after adding 4-dimethylaminopyridine (2.31×10^{-4} M), a highly efficient catalyst, the mixture was allowed to stand at room temperature until esterification was complete. Product **1**, further purified by reversed-phase HPLC (eluent water–acetonitrile–triethylamine–acetic acid), was obtained in 70% yield.

Enzyme inhibition in vitro. All reagents were purchased from Sigma Chemical (St. Louis, MO, USA). AChE activity from the electric eel (type V-S, E.C.3.1.1.7) was determined by the Ellman method. The assay medium contained the substrate acetylthiocholine iodide (0.33–1.7 mM), dithiobisdinitrobenzoic acid (0.5 mM), AChE 0.5 (EU ml^{-1}) and sodium phosphate buffer (0.1 M, pH 7.4). The reaction was monitored at 412 nm and 25 °C with a Pye Unicam SP8–250 UV–visible spectrophotometer using thermostated cells. The Michaelis–Menten constant (K_M) was determined using graphic fitting software (Kaleidagraph). Each experiment was repeated three times. Samples assayed in the absence of inhibitor served as controls. The inhibition competitive constant K_i was determined for **1** from the relationship between K_i and the concentration of inhibitor that causes 50% inhibition (IC_{50}) of the competitive enzymatic reaction, according to the equation $IC_{50} = K_i\ (1 + [S]/K_M)$. Dilution test: conditions before dilution in the absence or in the presence of inhibitor: $[E_{tot}] = 0.5$ EU ml^{-1} and $[S] = 2.5 \times 10^{-4}$ M; $[I] = 1\ \mu m$.

NMR measurements. The purity (>99%) of **1** was checked by HPLC. AChE from electric eel was used without further purification. Solutions were prepared in 100% deuterium oxide (Euriso-top, CEA, Saclay, France) buffered at the physiological pH (phosphate buffer, 0.1 M $Na_2HPO_4 + 0.1$ M NaH_2PO_4, pH* = 7.4). All NMR experiments were carried out at 500.11 MHz for ^1H and 125.027 MHz for ^{13}C and at 298 and 303 ± 1 K on a Bruker DMX spectrometer equipped with a 5 mm Z-

gradient reverse probe and a Silicon Graphics workstation. Chemical shifts were determined relative to internal DSS (sodium 2,2-dimethyl-2-silapentane-5-sulfonate).

For 1D ^{1}H NMR, FIDs were acquired over 5 kHz spectral width with 32K data points; exponential apodization gave 1 Hz line broadening. Suppression of water resonance was achieved by low-power irradiation during the relaxation delay (2 s), with an attenuation of 60 and 55 dB in the absence and the presence of the enzyme, respectively.

A 2D COSY[23] experiment was acquired for **1** (1.2 mM) at 298 K using 256 t_1 increments with 2K data points and 128 scans each. Partial suppression of the residual HDO signal was accomplished by presaturating during the 1.5 s relaxation delay. The data were processed with a non-shifted sine-bell window in both dimensions.

The phase-sensitive gradient selective HSQC[24] and gradient-selected HMBC[25] (delay = 70 ms corresponding to ^3J(C,H) = 7 Hz) experiments were recorded at 298 K. These experiments were acquired using 256 t_1 increments with 2K data points and 64 scans (HSQC) or 128 scans (HMBC). Two zero-fillings were applied in the f_1 dimension and a $\pi/3$ shifted squared sine-bell function was used in both dimensions.

NOESY experiments were recorded using standard techniques with the time-proportional phase incrementation mode (States-TPPI) with pulse sequence of Otting *et al.*[26] Suppression of the water resonance was achieved by presaturating during the relaxation delay. The 2D NOESY experiment for **1** (1 mM) in the absence of AChE was acquired with a mixing time of 1 s and a relaxation delay set to 1.1 s. The data matrix of 2K × 256 points was processed using a shifted sine-bell window function ($\pi/2$) in both dimensions with zero filling in f_1 to 2K × 1K.

From the technical point of view, attention was carefully paid to the spin-diffusion effect. The line broadening of **1** was proportional to the amount of AChE. A low enzymatic concentration (2.24 μM) with a large concentration of ligand (1 mm) caused a half line broadening of **1** signals. Under these conditions, (ratio R = [ligand]/[enzyme] = 446), the TrNOE cross peaks were well resolved. At higher concentrations of **1**, the resonances of H1, H8 and H3, H6 overlapped. On increasing the concentration of AChE (ratio $R \leq 66$), strong spin diffusion effects were observed for all protons of bound ligand.

Initially, transferred NOEs were measured with a wide range of NOE mixing time, τ_m (50, 65, 80, 100, 150 and 300 ms), for a ratio R = [ligand]/[enzyme] = 223 (concentration of **1** = 0.5 mM, concentration of enzyme = 2.24 μM) to determine the optimized value of τ_m. For τ_m = 50 ms, TrNOEs were scarcely detectable. Notable spin diffusion effects appeared for mixing times >100 ms. In consequence, it was not possible, in this study, to obtain NOE build-up curves to evaluate the contribution of diffusion spin. Then, TrNOESY experiments were performed and compared using an identical mixing time (τ_m = 65 ms, which gave a reasonable experimental signal-to-noise ratio) with various ratios R = 223, 446 and 892. For each case, the intensities of the detected transferred NOEs were measured. The results showed that, for each cross peak, the relative intensities of transferred NOEs determined with respect to the reference cross peak (H1′, H2′) were similar (±20%) in the three experiments. Finally, a TrNOESY experiment from the inhibitor–enzyme complex to the free inhibitor was performed at 303 K under conditions that insured the best signal-to-noise ratio and very limited spin diffusion. The enzyme concentration was 2.24 μM and the [ligand]/[AChE] ratio was 446. FIDs were acquired using a mixing time of 65 ms. A total of 320 incremental values of the evolution time were used with 320 scans, 2K data block over 5000 Hz and a relaxation delay of 1.1 s. Appropriate zero filling was carried out to yield a final two-dimensional matrix of 2K × 1K real points. A 60° shifted squared sine-bell was applied in both dimensions. The final matrix was baseline corrected separately on each side of the water signal in the f_2 dimension with a third-order polynomial.

Supplementary material

The Supplementary material available at the epoc website in Wiley Interscience contains the NOESY spectrum of **1** (1 mM, pH* 7.8, 303 K) at 500.11 MHz, with a mixing time of 1 s and the TrNOESY spectrum of **1** (1 mM, pH* 7.8, 303 K) in the presence of AChE (2.24 μM) at 500.11 MHz, with a mixing time of 65 ms.

REFERENCES

1. Ronzani N. *Analusis* 1995; **23**: 164–168.
2. Sussman JL, Harel M, Frolow F, Oefner C, Goldman A, Toker L, Silman I. *Science* 1991; **253**: 872–879.
3. Pomponi M, Marta M, Collela A, Sacchi S, Patamia M, Gatta F, Capone F, Oliviero A, Pavone F. *FEBS Lett.* 1997; **409**: 155–160.
4. Brufani M, Marta M, Pomponi M. *Eur. J. Biochem.* 1986; **157**: 115–120.
5. Harel M, Schalk I, Ehret-Sabatier L, Bouet F, Goeldner M, Hirth C, Axelson PH, Silman I, Sussman JL. *Proc. Natl. Acad. Sci. USA* 1993; **90**: 9031–9035.
6. Carlier PR, Han YF, Chow ES-H, Li CP-L, Wang H, Lieu TX, Wong HS, Pang Y-P. *Bioorg. Med. Chem.* 1999; **7**: 351–357.
7. Carlier PR, Du D-M, Han YF, Liu J, Pang Y-P. *Bioorg. Med. Chem. Lett.* 1999; **9**: 2335–2338.
8. Han YF, Li CP-L, Chow E, Wang H, Pang Y-P, Carlier PR. *Bioorg. Med. Chem.* 1999; **7**: 2569–2575.
9. Ni F. *J. Magn. Reson. B* 1995; **106**: 147–155.
10. Schwarz G, Alberts H, Kricheldorf HR. *Liebigs Ann. Chem.* 1981; 1257–1270.
11. Hassner A, Alexanian V. *Tetrahedron Lett.* 1978; **46**: 4475–4478.
12. Inanaga J, Hirata K, Saeki H, Katsuki T. *Bull. Chem. Soc. Jpn.* 1979; **52**: 1989–1993.

13. Ellman GL, Courtney KD, Andres V Jr, Featherstone RM. *Biochem. Pharmacol.* 1961; **7**: 88–95.
14. Michaelis L, Menten ML. *Biochem. Z.* 1913; **49**: 333–369.
15. Lineweaver H, Burk D. *J. Am. Chem. Soc.* 1934; **56**: 658–666.
16. Fersht A. *Enzyme Structure and Mechanism* (2nd edn). Freeman: New York, 1985.
17. Craig N, Newton J. Cumulative Subject Index and Drug Compendium. In *Comprehensive Medicinal Chemistry*, vol. 6, pp 269 and 878, Hansch C, Sammes PG, Taylor JB (eds). Pergamon Press: Oxford, 1990.
18. Marta M, Castello C, Oliverio A, Pavone F, Pagella PG, Brufani M, Pomponi M. *Life Sci.* 1988; **43**: 1921–1928.
19. Swift TJ, Connick RE. *J. Chem. Phys.* 1962; **37**: 307–320.
20. Moore JM. *Biopolymers (Pept. Sci.)* 1999; **51**: 221–243.
21. Feeney J, Birdsall B. In *NMR of Macromolecules. A Practical Approach*, Roberts GCK (ed). Oxford University Press: New York, 1993; 183–215.
22. Wong DM, Greenblatt HM, Dvir H, Carlier PR, Han Y, Pang Y, Silman I, Sussman JL. *J. Am. Chem. Soc.* 2003; **125**: 363.
23. Derome AE. *Modern NMR Techniques for Chemistry Reasearch*. Pergamon Press: Oxford, 1991; 183–234.
24. Schleucher J, Schwendinger M, Griesinger C. *J. Biomol. NMR* 1994; **4**: 301–306.
25. Wilker W, Liebfritz D, Kesserbaum R, Bemel W. *Magn. Reson. Chem.* 1993; **31**: 287–292.
26. Otting G, Widmer H, Wagner G, Wüthrich K. *Magn. Reson.* 1986; **66**: 187–193.